AN ESR STUDY OF $Mg_2P_2O_7:Mn^{++}$

AN ESR STUDY OF $Mg_2P_2O_7$:Mn^{++}

BY

LEUNG JURN SUN B.Sc.

A Thesis
Submitted to the Faculty of Graduate Studies
in Partial Fullfillment of the Requirements
for the Degree
Master of Science

McMaster University
October, 1964

MASTER OF SCIENCE (1964)
(Physics)

McMASTER UNIVERSITY
Hamilton, Ontario

TITLE: An ESR Study of $Mg_2P_2O_7$:Mn^{++}

AUTHOR: LEUNG JURN SUN B.Sc. (Chung Chi College, The Chinese University of Hong Kong)

SUPERVISORS: Professors C. Calvo, W. R. Datars

NUMBER OF PAGES: V, 60

CONTENT: Single crystals of $(Mg_{99.75}\ Mn_{0.25})_2\ P_2O_7$ have been investigated by esr through the temperature range from room temperature to 200°C. One phase transition was observed extended through the temperature range between 59.5 to 63°C where the α-and β phase coexist. Accurate spectra were recorded at 74°C, 84°C and 94°C at the three magnetic axis, and the spin-Hamiltonian parameters were obtained from these data. The phase transition mechanism and the significance of the spin-Hamiltonian parameters in the theory of S-state splitting are discussed in the light of current literature.

ACKNOWLEDGEMENTS

The author wishes to express his sincere gratitude to Professor W. R. Datars for his guidence and help throughout the course of this research. His gratitude is also due to Professor C. V. Stager for his generosity in his experience in microwave spectroscopy. Thanks are also extended to Mr. J. P. VanNest who had helped with recording of some of the data.

Especially, the author wants to thank Professor C. Calvo, who suggested the problem, who has drawn the authors attention to many of the references and whose discussions are stimulating in many ways.

This research is made possible through the support of the Ontario Research Foundation.

TABLE OF CONTENTS

ILLUSTRATIONS

TABLES

CHAPTER 1

Introduction

Phase transitions are observed in the sense that differential thermal analysis experiments showed endothermic or exothermic changes in the crystals of pyrophosphates of Cu, Mg and Zn[32]. Further experiments indicate that two phase changes occur in the latter two compounds. These occur at different temperatures, yielding the same ultimate high temperature forms although the room temperature phases are different. One of the major features in any attempt to predict statistically, from a molecular model, the nature of the phase transition, is the thermodynamic order of the change. It appears that we find both 1st and 2nd order phase transitions in this series. Any phase change in a crystal must be due to some structural rearrangement which minimze the Gibb's function of the body, and this depends on the energy correlation between the atoms at their specific sites and the thermal energy in the whole crystal. Since the high temperature phases of these pyrophosphates are isomorphic and their low temperature phases are closely related, the inevitable though complicated questions are what is the nature of the phase transition and what are the roles played by these cations in the mechanism of phase transitions? More precisely, what is the nature of the bondings that exist between them and their neighbouring atoms and what influence do they have on the bonding between the atoms of pyrophospate ion? Hence it is desirable to probe into the environment of these cations in their respective crystal sites and to trace any change of their environment with temperature. The esr technique is a good probe because of its sensitivity, though the need for a dilute paramagnetic ion substitution of the cation sites brings in modifications in their environment. $Mg_2P_2O_7$ is of special interest because measurements of thermodynamic potential reveals a first order phase transition at 68°C accompanied by an enthalpy change of 729 cal/mole while its specific heat follows a λ curve typical of continuous transition in second order.[33] Mn^{++} was used as the paramagnetic probe because its spectra is very sensitive to environmental change and $Mn_2P_2O_7$ is isostructural to β-$Mg_2P_2O_7$. We shall see that in our experiments, the transition temperature occurs lower by 8°C than it was previously reported. We also found evidence for a possible coexistance of two phase in a finite range of temperature.

On the other hand, the phenomenon of S-state splitting has always been a problem to esr investigators. All proposals for a mechanism have as yet reach no satisfactory conclusion. Some approximate theories on the value of D versus and axial crystal field are available, while the exact relation is still unknown.[10,12] One motive for this investigation is to add sufficient data in order that a definite answer may be given to this problem. The concept of spin-Hamiltonian has been very successful as far as intepretation of data is concerned, but discrepancy has been reported when the experimental data is fitted to the spin-Hamilton derived by peturbtion methods. Its derivation from perturbation methods depend on certain assumptions which are not defectless. This is discussed in

Chapter II, but the results of this present research do not permit us to test the additional terms.

CHAPTER 2

Theory

1. Paramagnetic Ions and ESR

A paramagnetic ion is one that exhibits non-zero angular momentum and hence a magnetic moment which is parallel to the former. Such ions have non-paired electrons because of incompletely filled inner shells. Classically, such a system will precess with Larmor frequency ω about an applied magnetic field. A circularly polarized electro-magnetic radiation field of frequency ω applied perpendicular to $\vec{H}$ will exert a couple on the angular momentum vector and reverse its direction. The result is an exchange of energy between the ion and the radiation field. From a quantum mechanical point of view, the additional energy operator $\mathcal{E} = -\vec{\mu}\cdot\vec{H}$ (which is equal to $\alpha\ \vec{J}\cdot\vec{H}$ where α is a constant), due to the interaction between the applied field and the magnetic moment of the ion causes Zeeman splittings among energy eigenstates with different magnetic quantum number M. The radiation field induces magnetic dipole transitions between these magnetic sublevels with selection rule $\Delta M = \pm 1$. For two specific levels, the probabilities of $\Delta M = -1$ and $\Delta M = +1$ transitionsare identical but the population of these states are different at ordinary temperature, since the distribution is determined by the thermal energy available. Therefore, in the radiation field there will be a resultant absorption of energy which can be detected experimentally. The equation describing this exchange of energy is $h\nu = g\beta H$ where g is the spectroscopic splitting factor and β the Bohr magneton. For ordinary laboratory magnetic field ν of the radiation field falls within the microwave range.

2. The Spin-Hamiltonian by Perturbation Method

The Hamiltonian of a free ion with n electrons takes the form:

$$H = \sum_{i}^{n} \left(\frac{P_i^2}{2m} - \frac{Ze^2}{r_i} \right) + \sum_{i>j}^{n} \frac{e^2}{r_{ij}} + \sum_{i}^{n} \xi(r_i)\, \vec{l}_i \cdot \vec{s}_i + V_{ss} + V_N \qquad (1)$$

where $\vec{l}_i$ and $\vec{s}_i$ are the orbital angular momentum and spin vectors of the i^{th} electron, V_{ss} arises from spin-spin interaction and V_N from the magnetic and electrostatic interaction* between nucleus and electrons. These terms occur roughly in the order of decreasing magnitude and the last three terms are ordinarily treated as perturbations. The inter-electronic Coulombic term prevents the Schrodinger equation from being separated while it itself is too large to be adequately treated as a pertubation for the 3d transition metal ions. Also, the effect of the complete shells is to provide an approximately spherically symmetric potential for the electrons in incomplete shells, and these electrons are the important ones in esr experiments. We therefore replace the first three terms by the Hamiltonian

$$H_o = \sum_{i}^{n'} \frac{P_i^2}{2m} + U(r_i) + H_1$$

---

* of order equal to or higher than four.

where the summation is carried over the electrons in the incomplete shell only, $U(r_i)$ is a single electron operator and $H_1 = \sum_{i=1}^{n} (\frac{-Ze}{r_i} - U(r_i)) + \sum_{i>j}^{n} \frac{e^2}{r_{ij}}$ is to be treated as a perturbation. With the first two terms of H_o, the Schrodinger equation is resolved into single electron equations. The angular part of the solutions to these equations are the familiar spherical harmonics while the orbital part is determined by the detail nature of $U(r_i)$. The zero order eigenkets of H_o with H_i considered as a perturbation are therefore determinental products of single electron orbital with appropriate spin functions and characterized by quantum numbers n, ℓ, m_ℓ, m_s. The energy of these so called Slater determinent is highly degenerate. To impose the perturbation of H_1, for which we assume the inequality $H_1 \gg \sum_i^n \xi(r_i)\, \vec{\ell}_i \cdot \vec{s}_i$, we first note that the two terms in the bracket only produce a uniform shift of energy in one configuration and therefore can be neglected if we confine our interest to a single configuration. To evaluate the matrix of $\sum_{i>j}^{n} \frac{e^2}{r_{ij}}$ in all determinental product states is both tedious and unnecessary. Noting that this operator commutes with both L and S, the total orbital angular momentum and spin operators respectively, we can select, according to Hund's rule, all the appropriate $|LM_LSM_S\rangle$ kets which are possible for the configuration in question. The possible energy eigenvalues are given by the diagonal matrix of H_1 in these kets. To evaluate these matrix elements $\langle LM_LSM_S | H_1 | LM_LSM_S\rangle$ we can again express $|LM_LSM_S\rangle$ in terms of linear combination of products of single electron orbitals and perform the integration involving the two particle operator. The result is expressible in terms of the experimentally adjustable Condon-Shortley-Stater Coefficients because $U(r_i)$ is not known.[1] The spin-orbit term does not commute with $\vec{L}$ and $\vec{S}$ separately, but if its magnitude is small, the coupling effect may be neglected. Its effect will then be to raise the J degeneracy and split the term corresponding to the kets $| LM_L SM_s \rangle$ according to Lande interval rule which states that $E(J) - E(J-1) = \lambda J$ where $E(J)$ is the energy of the state characterized by total angular momentum J and λ is a constant for the ion. However, if on the other hand this term is prominent, L and S will no longer be good quantum numbers and the so called j-j coupling is a better approximate.

Once the ion is embedded in a crystal, its Hamiltonian in principle containsterms in the sum for every electron and nuclei. As far as esris concerned, the effect of the crystal surrounding can be well accounted for by an inert electrostatic crystal field at the paramagnetic ion, characterized by the symmetry of the latter's immediate locality but with no electron mixing at the paramagnetic ion. This is equivalent to reducing the crystal environment to fixed point charges properly places around the paramagnetic ion. The crystal field term, V_F, in the Hamiltionian may be expressed as a series of normalized spherical harmonic multiplied by some radial functions i.e.,

$$V_F = \sum_i \sum_\ell \sum_m Y_\ell^m (\theta_i \varphi_i) R_{n\ell}(r_i), \qquad (2)$$

since these functions form a complete set. This form for V_F is valid at every point inside a sphere whose radius is the distance from the nearest ligand with the paramagnetic ion excluded, **where it is a well behaved** function of the position coordinates. V_F must be invariant under the transformation group of the ion's locality. Furthermore, to evaluate the angular part of matrix elements of V_F in any manifold reduces to calculation of integrals of tensor operators between single electron orbitals with well defined angular momentum, i.e. ket product of the form $\langle n\ell m_\ell m_s | Y_L^M | n'\ell' m_\ell' m_s' \rangle$ and these matrix elements vanish unless the triangular rule $|\ell-\ell'| \leqslant L \leqslant \ell+\ell'$ is satisfied. Hence terms in Y_L^M for which L exceeds 2ℓ can make no contribution when we consider electrons in a shell of angular momentum ℓ. These facts greatly reduced the number of terms that need to be considered in V_F. Usually, group theoretic considerations enables one to determine entirely the angular dependence of V_F provided the point group at the ion is known.[2]

For the 3d electrons of the ion transition group. The magnitude of V_F usually falls between the pairing energy and spin-orbit coupling energy. Since the spherical symmetry of the free ion Hamiltonian is destroyed by the crystal field, the states are no longer pure $|LM_L SM_S\rangle$ states. However, appropriate symmetrized states can be constructed from linear combinations of these with the help of group theory. We can then employ the operator equivalent method,[5] which is a straight forward application of Wigner-Eckart theorem (and which itself follows directly from Schur's lemma)[3,4], to cast V_F into a polynomial of components of angular momentum operators for the specific configuration of equivalent electrons. What we really want to do is to replace the tensor operators $\sum_{L,M} Y_L^M$ by a polynomial in L_x, L_y and L_z, which transforms similarly to the former, and Wigner-Eckart theorem guarentees the possibility of this. In practice, to do this in an L-manifold, we can either replace M_L by L_z in the 3-j symbol at the right hand side of the matrix element

$$\left\langle LM_L \middle| Y_\ell^q \middle| LM_L - q \right\rangle = (-1)^{L-M_L} \begin{pmatrix} L & \ell & L \\ -M_L & q & M_L-q \end{pmatrix} \left\langle L \middle\| Y_\ell^{\,q} \middle\| L \right\rangle$$

or by replacing x, y and z in $\sum_{LM} Y_L^M$ by the operators L_x, L_y and L_z, taking care about the fact that L_x, L_y and L_z are not mutually commuting as the position coordinates were. When this is done, the angular contribution of energy eignvalue of V_F can be integrated without much difficulty.

The Electron Spin Resonance technique allows one to determine the transition energies between Zeeman splittings of the ground level of these "crystal field states". Of course the perturbation effects of those terms so far deleted from H also appear in the spectra. The part of Hamiltonian that remains to be dealt with is $H' = -\vec{H}\cdot(\vec{L} + 2\vec{S}) + \sum_i \zeta(r_i)\,\vec{\ell}_i\cdot\vec{s}_i + V_{ss} + V_N$. To carry out this perturbation, the following transformation is made, again with the help of operator equivalent method,

$$H' \longrightarrow P(L_x, L_y, L_z, S_x, S_y, S_z, I_x, I_y, I_z).$$

where P is a polynomial and S_x and I_x and etc. are the spin and nuclear spin operators respectively. Then a formal perturbation of second order is carried out for P in the L-manifold, treating the spin and nuclear variables as non-commuting algebraic quantities. The result is not the energy eigenvalue of H', but an expression $H_s(S_x, S_y, S_z, I_x, I_y, I_z)$ involving as variables the spin and nuclear operators only. The terms of such a spin-Hamiltonian can be summarized as

$$H_s = \beta\vec{H}.\vec{g}.\vec{S} + \vec{S}.\vec{D}.\vec{S}. + \vec{I}.\vec{A}.\vec{S}. \qquad (3)$$

where $\vec{g}$, $\vec{D}$ and $\vec{A}$ are symmetric tensors[6,7]. These three terms describe respectively the Zeeman splitting, the zero-field splitting due to spin orbit coupling and the hyperfine splitting. Since the components of these tensors in this approximation arise from integration like $\langle n | L_i | n' \rangle$ where the eigenkets are symmetrized crystal field states, we expect them to reflect the symmetry of V_F. The spin-Hamiltonian concept permits the paramagnetic resonance problem to be resolved into one mainly concerned with determining the spin-Hamiltonian parameters from experimental data. It is still necessary, of course, to construct a satisfactory model of the crystal field so that the spin-Hamiltonian parameters can be expressed in terms of integrals involving one or two particle operators acting on single electron orbitals.

3. The S-State, Line Positions of Mn^{++}

The ground state of Mn^{++} is a $3d^5$ ^6S 5/2 state. It is already split into a Γ_7 doublet and a Γ_8 quartet in a cubic field. Further splitting can occur for a still lower site symmetry. In our case we have three Kramers doublets with the absence of a magnetic field, yet if we use the perturbation method above these states have to be accidentally degenerate.

Because the d^5 configuration is a complimentary to itself, it cannot be split by a crystal field that satisfies Laplace's equation.[8] On the other hand, first order spin-orbit coupling does not lift the six-fold degeneracy because an S state ion forms, under all symmetry operation, a basis for the identical representation Γ_1 while the angular momentum vector never takes this representation except for spherical symmetry which we assumed to have been destroyed by the crystal field from the start. Thus no non-vanishing integral can be formed from products of functions tranforming as indicated. In fact, it has always been found that Mn^{++} ground state is split into three Kramers doublets with considerable zero field splitting. (Fig. 1) To give account for this, various detailed second or higher order processes have been proposed. Pryce had suggested that the spin-spin magnetic dipole interaction is prominent because of distortions of the electron cloud from spherical symmetry.[9] Watanabe had considered simultaneous crystal field and spin-orbit coupling between the S state and other excited quartet and sextets arising from the d^5 configuration[10]. Gabriel et al have considered all the 252 spin-multiplets of the d^5 configuration, using the Hamiltonian

$$H = T + V + \sum_{i>j} \frac{e^2}{r_{ij}} + \sum_i V_i + \sum_i \xi(r)\, \vec{l}_i \cdot \vec{s}_i + W_{ss}$$

where T is the kinetic energy term and V the spherical symmetric potential due to the argon core and V_i the crystal field acting on the i^{th} electron[11]. None of these proposals seemed definitive and the real mechanism has not yet been clarified.

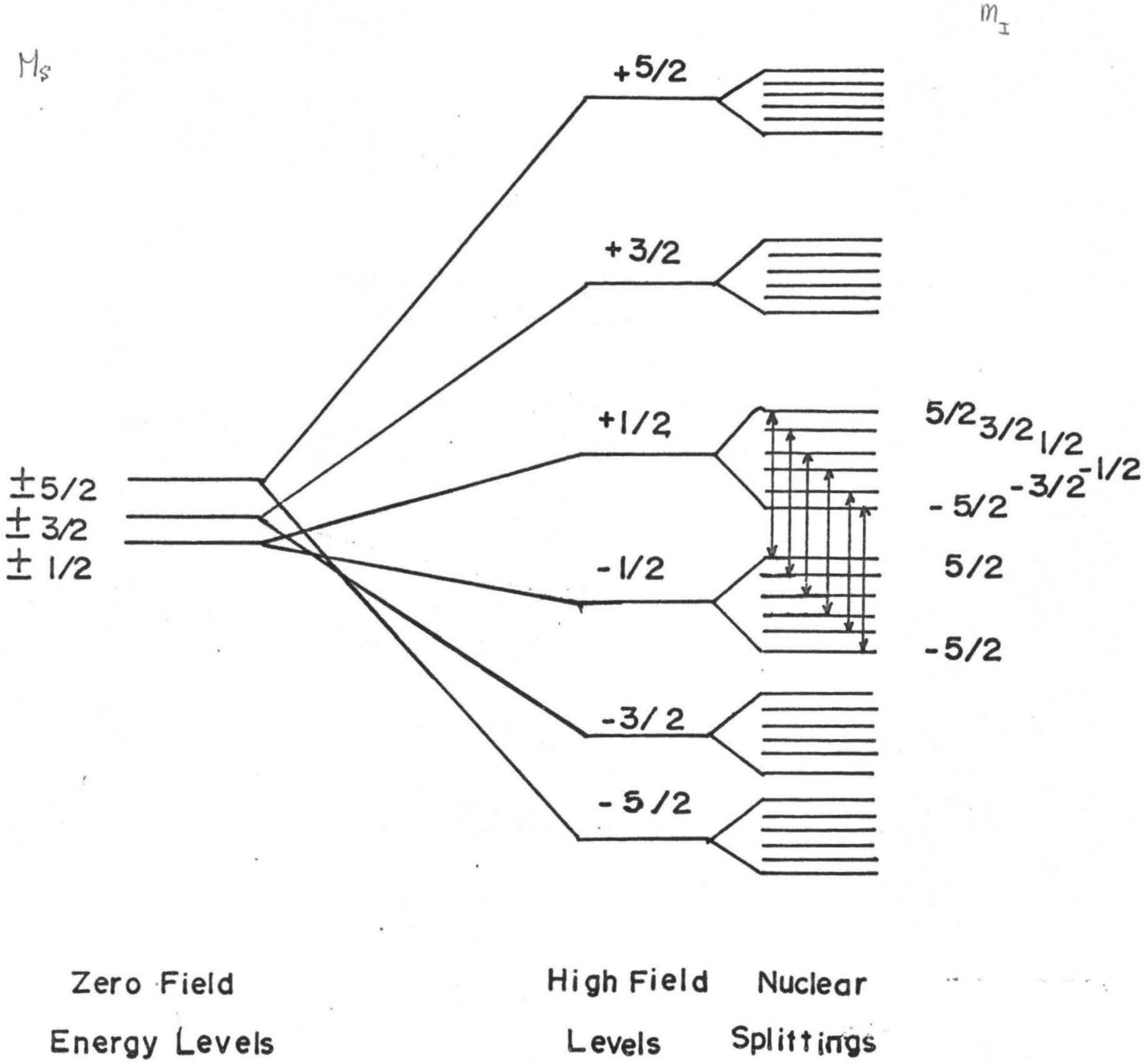

Fig. 1 Schematic Energy Level Diagram of Mn++
(After B.Bleaney & D.J.E. Igram, 1951)

Efforts have been made to investigate the relation between the zero field splitting parameter D and the axial field component Y_2^o in the expression of V_F. It is conjectured that their relation is of the form $D = C_1 Y_2^o + C_2 Y_2^{o2}$. But neither the magnitude nor the signs of the parameters C_1 and C_2 has been satisfactorily worked out[12].

Furthermore, no hyperfine structure is expected for an S-state ion for, with L = 0, the interaction between nuclear and electron spin averages to zero. However, large hyperfine interaction has always been detected. Abragam proposed that this may be explained by the coupling of the $3d^5\ {}^6S5/2$ state with a state with configuration $3d^5 4s$ in which an s-electron from an inner shell is promoted to the n = 4 shell[13]. Heine[14] and also Wood and Pratt[15], tried to explain this effect by the exchange polarization of the completed s-shells. Because all the d-electrons are lined up as predicted by Hund's rule, the inner electrons will see a large spin polarization and the restricted Hartee-Fock approximation, in which electrons with equal n and ℓ quantum numbers are assigned identical wave function, is no longer adequate. This is because the electrons with spins **parallel** to those of the d-electrons will have an extra exchange interaction stabilization over the electrons which are antiparallel.

To circumvent these difficulties when the perturbation method is applied to an S-state ion, the spin-Hamiltonian is obtained by writing out a polynomial of even powers of components of $\vec{S}$, which satifies the symmetry requirement of the **paramagnetic** ion's locality, and to which are added the tensor operators $\overline{H}\cdot\overline{S}$ and $\overline{I}\cdot\overline{S}$ that yield the Zeeman and hyperfine terms. The number of undetermined parameter in these operators depends on the point group and the ground state in question[7,16]. The generally used spin-Hamiltonian for Mn^{++} is

$$H = g\beta\overline{H}\cdot\overline{S} + DS_z^2 + E(S_x^2 - S_y^2) + A\ \overline{I}\cdot\overline{S} \tag{4}$$

If we use the above spin-Hamiltonian, perturbation to third order shows that the fine structure positions for magnetic field along the z-axis are:

$$H_{\pm\frac{5}{2}\longleftrightarrow\pm\frac{3}{2}} = H_o \mp 4D + \frac{4E^2}{H_o} \pm \frac{6DE^2}{H_o^2} \tag{5.1}$$

$$H_{\pm\frac{3}{2}\longleftrightarrow\pm\frac{1}{2}} = H_o \mp 2D - \frac{5E^2}{H_o} \pm 33\frac{DE^2}{H_o^2} \tag{5.2}$$

$$H + \frac{1}{2}\longleftrightarrow -\frac{1}{2} = H_o - \frac{8E^2}{H_o} \tag{5.3}$$

where $H_o = \frac{h\nu}{g\beta}$, ν being the microwave frequency[17]. Chambers in his study of $Zn_2P_2O_7$:Mn^{++} has carried through the perturbation to the fourth order[18]. These terms make significant contributions when D is large. The additional terms are

$$H_{\pm\frac{5}{2}\longleftrightarrow\pm\frac{3}{2}} : \frac{36\ D^2E^2}{H_o^3} + \frac{28\ E^4}{H_o^3} \tag{6.1}$$

$$H \pm \frac{3}{2}\longleftrightarrow\pm\frac{1}{2} : \frac{45\ D^2E^2}{H_o^3} - \frac{5}{4}\ \frac{E^4}{H_o^3} \tag{6.2}$$

$$H_{\pm\frac{1}{2}\leftrightarrow-\frac{1}{2}}: \quad \frac{72\ D^2E^2}{H_o^3} + \frac{56\ E^4}{H_o^3} \tag{6.3}$$

The simple substitutions for

$$H /\!/ X \text{ of } D \Rightarrow \frac{1}{2}\ (3E-D),\ E \Longrightarrow -\frac{1}{2}\,(E + D) \tag{7.1}$$

and for $$H /\!/ y \text{ of } D \Rightarrow -\frac{1}{2}\ (3E+D),\ E \Longrightarrow \frac{1}{2}\,(D - E) \tag{7.2}$$

transforms the expressions (5) and (6) to those describing the situation where magnetic field is parallel to the other axes.

The hyperfine structure is found to be nearly isotropic. Its effect to the 2nd order is accounted for by the addition of the following terms to the transition between states with magnetic spin quantum number M_s and M_s-1:

$$-Am_I - \frac{A^2}{2H_o}\ \left(\frac{35}{4} - m_I^2\right) - \frac{A}{2H_o}\ (2M_S - 1)m_I \tag{8}$$

where m_I is the nuclear spin magnetic quantum number. The selection rule for this quantum number is $\Delta M_I = 0$[19].

4. Energy Levels By Group Theoretic Approach

The perturbation method described above depends on the assumptions that the inequalities $\sum_{i>j}^{n} \frac{e^2}{r_{ij}} \gg V_F \gg \sum_{i}^{n} \xi(r_i)\ \vec{l}_i\cdot\vec{s}_i$ hold and that the ground state of the paramagnetic ion is non-degenerate in the crystal field. As we see, it breaks down altogther for an S-state ion. The crystal field approximation also exclude electron exchange between the paramagnetic ion and its neighbouring atoms. Koster and Statz[20] reported a method which requires a much less stringent condition. Their method is essentially a natural extension of the Wigner-Eckart theorem. The Wigner-Eckart theorem deals with eigenkets and tensor operators which transform irreducibly under the full rotation group, i.e. the J-manifolds and spherical harmonic operators and structures isomorphic to them[21]. It states that the integral of an irreducible tensor operator between two states of defined J is the product of a reduced matrix element and a Clebsh-Gordon coefficient. There exists a similar relation between kets and operators which transform irreducibly under other groups, and in this case, the symmetry group of the paramagnetic ion. The integral of such operators between such eigenkets involves some coefficients which behave very similarly to the Clebsh-Gordon coefficients and need be evaluated once.

Let us write the Hamiltonian as $H = H_o + H_1$ where H_o includes all contributions to energy, and hence also any bonding effects present, except interaction with the magnetic field. Therefore, $H_1 = g\beta\vec{H}.(\vec{L} + 2\vec{S})$. If E_α, E_β and E_n are the energy eignevalues of H_o, the degeneracy of their corresponding eigenkets $\langle\alpha|$, $\langle\beta|$...and $\langle n|$ is determined by the branchings of the free ion states under the symmetry group G of H_o. The n_α fold degenerate eigenkets $\langle\alpha_1|$, $\langle\alpha_2|\cdots\langle\alpha_{n_\alpha}|$ form a basis of a certain irreducible representation of G. To be explicit, if K is an element of G and Γ_α and Γ_β are some irreducible representations of G, we have

$$K|\alpha_i\rangle = \sum_{m=1}^{n_\alpha} U_\alpha(K)_{mi} \; |\alpha_m\rangle$$

and $$K \left| \beta_j \right\rangle = \sum_{n=1}^{n_\beta} U_\beta (K)_{nj} \left| \beta_n \right\rangle \tag{9}$$

We now calculate the perturbation of H_1 on these exact eigenkets of H_o. The ones of interest to esr are the very lowest groups. Usually one can make use of the fact that the energies of higher configurations are remote with respect to the ground state energy and therefore the number of states that need to be considered is not very large. And, in any case, our error can be made as small as desired by taking sufficiently large number of states. The next step is to break up H_1 into a sum of operators transforming irreducibly under G, i.e. to write

$$H_1 = \beta \sum_{\gamma,k} H_\gamma^{\,k} (L + 2S)_\gamma^{\,k} \tag{10}$$

and $(L + 2s)_\gamma^{\,k}$ is the k^{th} partner of the γ irreducible representation of G. The matrix elements can be easily obtained. Thus

$$\left\langle \alpha_i \left| \sum_k H_\gamma^{\,k} (L + 2s)_\gamma^{\,k} \right| \beta_j \right\rangle = \sum_{\ell}^{N_\ell} g_{\gamma,\ell}^{\alpha\beta} \sum_k H_\gamma^{\,k} U_{k,ij}^{\ell}$$

where N_ℓ is the number of times $\Gamma_\gamma^{\,*}(G)$ appears in $\Gamma_\alpha^{\,*}(G) X \Gamma_\beta(G)$. N_ℓ is the number of independent parameters that appears in the $\alpha\beta$ block of our $\sum n_\alpha \; x \sum n_\beta$ matrix. The summation is to be carried through all the groups of degenerate eigenkets we have considered. The U's are the coefficients of the transformation

$$\left| \gamma_{k\ell} \right\rangle = \sum_{i,j} U_{k,ij}^{\ell} \left| \alpha_i^* \right\rangle \left| \beta_j \right\rangle \;^{+} \tag{11}$$

+ $\left| \alpha_i^* \right\rangle$ is a basis ket of the representation $\Gamma_\alpha^{\,*}$

The effective symmetry group of Mn^{++} in $Mg_2P_2O_7$ is C_{2v}. Its character table as a double group is given below along with the bases for the various irreducible representations[22].

	E	C_2	v	v'	Bases
Γ_1	1	1	1	1	Z
Γ_2	1	-1	1	-1	X or Sy
Γ_3	1	1	-1	-1	Sz or Xy
Γ_4	1	-1	-1	1	Sx or Y
Γ_5	2	0	0	0	$\emptyset(\frac{1}{2}, \frac{1}{2}), \emptyset(\frac{1}{2} - \frac{1}{2})$

The ground state of Mn^{++} is $^6S5/2$. The characters of the representation, X(R), employing these six degenerate spin functions as a basis, can be obtained from the equation

$$X(R)_{5/2} = 2\ \mathrm{coz}(\tfrac{5}{2}\ \emptyset) + 2\ \mathrm{coz}(\tfrac{3}{2}\ \emptyset) + 2\ \mathrm{coz}(\tfrac{1}{2}\ \emptyset).$$

They are

	E	C_2	v	v'
X	6	0	0	0

Therefore

$$X(R)_{5/2} = 3\Gamma_5$$

Hence the $^6S5/2$ state branches into three Γ_5 doublets. These show Kramers degeneracy and therefore in this case time inversion symmetry does not add any further degeneracy. $L_x + 2S_x$, $L_y + 2S_y$ and $L_z + 2S_z$ are bases of representations Γ_4, Γ_2 and Γ_3 respectively of C_{2v}. The decomposition of the direct product $\Gamma_5^* \times \Gamma_5$ is as below:

$$\Gamma_5^* \times \Gamma_5 = \Gamma_1 + \Gamma_2 + \Gamma_3 + \Gamma_4$$

Since $\Gamma_5^* \times \Gamma_5$ contains all the three representations in H_1, three independent parameters appear in each 2 x 2 block and there are six independent blocks, therefore altogether 18 parameters are evolved from H_1. Two more parameters are needed to describe the energy separation between the three Γ_5 doublets at zero field. Hence in all 20 parameters are needed to describe the whole problem. To evaluate the complete matrix $H = H_o + H_1$, we have still to know the U's. They have been tabulated by Koster and Statz and given here below[22].

$$\begin{array}{cccc} \text{Operator} & L_y + 2S_y & L_z + 2S_z & L_x + 2S_x \\ \text{Matrix} & \begin{pmatrix} 0 & 1 \\ -1 & 0 \end{pmatrix} & \begin{pmatrix} 1 & 0 \\ 0 & -1 \end{pmatrix} & \begin{pmatrix} 0 & 1 \\ 1 & 0 \end{pmatrix} \end{array} \qquad (12)$$

Let E_1, E_2 be the energy separations between the two higher and the lowest Γ_5 doublets at zero-field, the complete matrix is

	$\Gamma_5^{a_1}$	$\Gamma_5^{a_2}$	$\Gamma_5^{b_1}$	$\Gamma_5^{b_2}$	$\Gamma_5^{c_1}$	$\Gamma_5^{c_2}$
$\Gamma_5^{a_1}$	$E_1 + a_3H_z$	$a_1H_x + a_2H_y$	a_yH_z	$a_4H_x + a_5H_y$	a_qH_z	$a_7H_x + a_zH_y$
$\Gamma_5^{a_2}$	$-a_1H_x + a_2H_y$	$-a_4H_z + E_1$	$-a_4H_y + a_5H_y$	$-a_6Hz$	$-a_6H_x + a_8H_y$	$-a_qH_z$
$\Gamma_5^{b_1}$			$E_2 + a_{12}H_z$	$a_{10}H_x + a_{11}H_y$	$a_{15}H_z$	$a_{13}H_x + a_{14}H_y$
$\Gamma_5^{b_2}$			$-a_{10}H_x + a_{11}H_y$	$E_2 - a_{12}H_z$	$-a_{13}H_x + a_{14}H_y$	$-a_{15}H_z$
$\Gamma_5^{c_1}$					$a_{18}H_z$	$+a_{16}H_x + a_{17}H_y$
$\Gamma_5^{c_L}$					$-a_{16}H_x + a_{17}H_y$	$-a_{18}H_z$

Usually consideration of the time inversion operator will reduce the number of independent parameters[22], though here this does not turn out to be the case because of the presence of Kramers degeneracy. But some insight into the nature of various parameters can still be obtained from such an investigation. The basis for Γ_5 in evaluating these matrices (12) are the spin functions $\emptyset(\frac{1}{2}, \frac{1}{2})$ and $\emptyset(\frac{1}{2} - \frac{1}{2})$. Let K be the time-reversal operator. Then,

$$\left\langle \alpha, \ \beta \right\rangle = \left\langle K\alpha, \ \ k\beta \right\rangle^{*}$$

and
$$K\ H_1\ K^{-1} = -H_1 . \qquad (13)$$

Now consider matrix element H_{24}

$$\left\langle (\alpha \tfrac{1}{2} - \tfrac{1}{2}) \right| H_1 \left| (\beta \tfrac{1}{2} - \tfrac{1}{2}) \right\rangle = \left\langle K(\alpha \tfrac{1}{2} - \tfrac{1}{2}) \right| K H_1 \left| (\beta \tfrac{1}{2} - \tfrac{1}{2}) \right\rangle$$

$$= \left\langle K (\alpha \tfrac{1}{2} - \tfrac{1}{2}) \right| K H_1 K^{-1} \left| K(\beta \tfrac{1}{2} - \tfrac{1}{2}) \right\rangle$$

$$= - \left\langle (\alpha \tfrac{1}{2} - \tfrac{1}{2}) \right| H_1 \left| (\beta \tfrac{1}{2} - \tfrac{1}{2}) \right\rangle^*$$

$$= -H_{13}{}^*$$

$$a_6 H_z = -a_6{}^* H_z$$

Hence a_6 is imaginary.

Similarly, for H_{23} we have

$$\left\langle (\alpha \tfrac{1}{2} - \tfrac{1}{2}) \right| H_1 \left| (\beta \tfrac{1}{2} - \tfrac{1}{2}) \right\rangle = - \left\langle (\alpha \tfrac{1}{2} - \tfrac{1}{2}) \right| H_1 \left| (\beta \tfrac{1}{2} - \tfrac{1}{2}) \right\rangle$$

$$-a_4 H_x + a_5 H_y = a_4{}^* H_x + a_5{}^* H_y$$

$$\begin{aligned} a_4 &= -a_4{}^* \\ a_5 &= a_5{}^* \end{aligned} \qquad (14)$$

Hence a_4 is imaginary and $a_5{}^*$ is real. Properties of other parameter can be obtained in the same way.

We shall remark in passing that the normal ESR technique does not allow us to measure all these twenty parameters.

5. Spin-Hamiltonian By Symmetry Considerations

The above analysis shows that more parameters than the conventional spin-Hamiltonian contains are needed to treat the effect of crystal field on a paramagnetic ion in a what we call an exact way. Grant et al[23] had reported in a recent paper that by way of tensor decomposition, a spin-Hamiltonian of sufficient parameters can be constructed. The most general form of the spin-Hamiltonian can be written as

$$H_s = \sum_{LM} a_{LM} \quad T_{LM}\,(\vec{H},\vec{S}) \tag{15}$$

where $T_{LM}(\vec{H}.\vec{S})$ is the Mth component of a L rank tensor operator. Since H_s has to be invariant under group G, determination of significant terms in the series as well as their coefficient a_{LM} can be achieved without ambiguity in the same manner as was the case of spherical harmonics of V_F. We then try to resolve the tensor operators T_{LM} that appear in H_s into products of other tensor operators that involve the field variable and the spin variable separately. The only additional equation we need is that expressing the coupling of two irreducible tensors to form a third one:

$$T_{LM}\,(\vec{V_1},\vec{V_2}) = \sum_{m_1} \left\langle \ell_1,\ell_2,m_1,m_2 \right| \left. LM \right\rangle T_{\ell_1 m_1}\,(\vec{V_1})\; T_{\ell_2 m_2}\,(\vec{V_2})$$

where ℓ_1 and ℓ_2 have to satisfy the triangular rule $|\ell_1 + \ell_2| \leqslant L \leqslant \ell_1 + \ell_2$ and $T_{\ell_1 m_1}$ and $T_{\ell_2 m_2}$ are tensors of rank ℓ_1 and ℓ_2 respectively. This decomposition is not unique. But further restrictions are provided by the facts that: (1) even rank spin tensors must be excluded because the requirement of time reversal symmetry (2) spin tensors of rank greater than 2S are excluded because all their matrix elements vanish and (3) only linear terms of the magnetic field tensor need be considered in the normal case. These enable us to perform the decomposition uniquely. The spin-Hamiltonian then takes the form

$$H_s = \sum_{\ell_1 \ell_2 m_1 m_2} C_{\ell_1 \ell_2 m_1 m_2} \; T_{\ell_1 m_1}(\vec{H}) \, T_{\ell_2 m_2}(\vec{S}) \tag{16}$$

The summation is taken of all possible decompositions of every $T_{LM}(\vec{H},\vec{S})$ subject to the above restrictions. The coefficients $C_{\ell_1 \ell_2 m_1 m_2}$ are not all independent. There still remains the problem of finding the explicit expression of the spin and field tensors involved. Luckily, they have been tabulated by Koster and Statz [20]. Grant et al had actually carried out the above procedure for an octahedral field and find the result similar to that derived by the method described in the previous section. Since here no other assumption is employed other than a knowledge of the symmetry group G, the aesthetic short comings of the perturbation method is avoided.

6. Second Order Phase Transition of Crystals

First order phase transition are said to occur at the discontinuity of $\nabla\Phi_{min}$. Such a point occurs where the Gibb's free energy function Φ_1 (P,T) and Φ_2(P,T) of two phases intersect. $\Phi_{min.}$ corresponds to the equilibrium state corresponding to a minimum in Φ, the Gibb's free energy function, at constant temperature and pressure.

Second order or λ transitions are characterized by a sudden change of symmetry but with no discontinuity of the thermodynamic state functions since the electron density is continuous across the transition. This is possible only if the symmetry of one phase is the subgroup of the other. Let G be the symmetry group at the transition temperature T_t and $\rho(x,y,z)$ the density function of the crystal. ρ can can be expanded uniquely as a linear combination of basis functions $f_i^{(n)}$ of irreducible representation Γ_n of G because they form a complete set. Denoting the part of this linear combination comprosed of basis function of Γ_1 as ρ_o, we may write $\rho = \rho_o + \eta$ with $\eta = \sum_{n, n\neq 1} \sum_i e_i^{(n)} f_i^{(n)}$. Clearly η cannot be identically zero in both phases else there will be no symmetry change at all. We therefore have $\eta_{T=T_t} = 0$ and $\lim_{T\rightarrow T_t} \eta = 0$. Hence Φ, being a continuous function of T, can be expressed in a power series of the coefficients $e_i^{(n)}$ $(n \neq 1)$ in the neighbourhood of T_t. In this expression, the linear term has to vanish because no linear combination of the $e_i^{(n)}$ $(n \neq 1)$ is invariant under G while Φ has to be invariant under all coordinate transformations. The second order term will not contain any cross term with different n because the direct product $\Gamma_n \times \Gamma_m$ does not contain Γ_1 unless n = m. Thus, to second order, $\Phi = \Phi(P,T) + \sum_{n \neq 1} A^n(P,T) \sum_i (e_i^n)^2$. Φ is a minimum at T_t where $e_i^n = 0$ if and only if $A^n(P,T) \geqslant 0$. Then, to have Φ still a minimum at a neighbouring points of T_t, in the phase with either symmetry without being reduced to the case where all $e_i^n = 0$, we require at least one, say A^m, to change sign at T_t. If this is the case, we have

$$A^n = 0, \quad e_i^m \neq 0 \text{ at where } A^m < 0 \quad \text{(unsymmetric phase).}$$

$$A^n \geqslant 0, \quad e_i^m = 0 \text{ at where } A^m \geqslant 0 \text{ (symmetric phase).}$$

and $e_i^n = 0$ for $n \neq m$.

Therefore our density function takes the form

$$\rho = \rho_0 + \sum_i e_i^m f_i^m$$

and has symmetry G for $A^m \geqslant 0$.

ρ has symmetry of $\sum_i e_i^m f_i^m$, i.e. of a subgroup of G for $A^m < 0$.

From the above results, the following properties of the function $\eta = \delta\rho(x,y,z) = \sum_i e_i^m f_i^m$ can be deduced:

$\eta = 0$ at T_t and in the symmetric phase where $A^m \geqslant 0$,

$\eta \neq 0$ but $\lim_{T \to T_t} \eta = 0$ in the unsymmetric phase where $A^m < 0$

η is a measure of the orderness of the system*.

---

* Of course the function of orderness of a system can take a much more general form than this, but it can always be related to ρ.

Φ is obviously a function of η and because of the above properties, an expansion of Φ in power series of η is possible.

$$\Phi = \Phi_o + \alpha\eta + A(PT)\,\eta^2 + \beta(PT)\,\eta^3 + C(PT)\,\eta^4 + \ldots\ldots\ldots$$

Here α has to vanish for the reason stated previously. Also $A(P,T)$ has to behave identically as $A^m(P,T)$ with respect to change of temperature. Therefore $A(P,T_t) = 0$. As an odd function cannot have a minimum at the origin, Φ can be maintained as a minimum in any neighbourhood of T_t only if $B(P,T_t) = 0$ and $C(P,T_t) = 0$. If $B(P,T)$ is not identically vanishing, the two conditions $A(P,T_t) = 0$ and $B(P,T_t) = 0$ give us, generally, a unique critical point. If on the other hand $B(P,T) \equiv 0$, the transition occurs along a transition curve of the form $T = f(P)$.

If an appropriate model is chosen, it can be shown that a discontinuity in specific heat does exist at T_t[24].

CHAPTER III

Crystallography and Phase Transition of $Mg_2P_2O_7$[25,26,27,31,32]

Phase transitions are observed in the series of pyrophosphates $Mg_2P_2O_7$, $Cu_2P_2O_7$ and $Zn_2P_2O_7$. The space groups of the β-phase of all three are C-2/m. In addition although $Mn_2P_2O_7$ at room temperature is isostructural to them, no phase transition in this compound has been detected above -60°C. The low temperature α-phase of $Zn_2P_2O_7$ appears to have a space group of symmetry I-c. This increases to C-m at 132°C through a first order phase transition where the c and a axes are halved and reduced to one third respectively. The symmetry is further raised at 155°C to C-2/m of the β-phase with no apparent volume discontinuity. This change is believed to be a second order transition. The phase transition of $Cu_2P_2O_7$ occurs at about 72°C and the α-$Cu_2P_2O_7$ has a space group C-2/c. The c-axis is halved through this transition.

$Mg_2P_2O_7$ is reported to undergo a first order transition at 68°C, with an enthalpy change 729 cal/mole, however the specific heat anomaly is spread over an interval of 20°C[33]. X-ray powder patterns indicate that two phases co-existed in this region[32]. Single crystal X-ray work shows that the transition temperature lies between 62°C to 65°C. Although the temperature is quite accurate there may be an error of about 2°C in the absolute value of the temperature. Both the c and a axes are halved. As in the other two compounds, b and β suffer no major change. The space group chosen for α-$Mg_2P_2O_7$ is $B\text{-}2_1/c$. In the temperature range of 62 to 65°C there appear to be two phases both apparently with the same X-ray extinctions. The nature of the symmetry change across this transition is not at all clear.

In β-$Mg_2P_2O_7$, the magnesium ion lies on a two-fold axis ligated with six neighbouring oxygens, forming a highly distorted octahedron. The major distortion is due to a rotation displacement of the O_{III}- O_{III}' pair and an elongation of the Mg - O_{III}'' bond. The three Mg - O bonds are 2.067Å, 2.005Å and 2.158Å respectively. The pyrophosphate ion form corner-shared tetrahedra. Infrared data shows that the central oxygen of a $P_2O_7^{-4}$ group undergoes enhanced thermal motion near 68°C and this is attributed to motion in the plane perpendicular to the P-P vector; the potential surface have at least two minima but above 68°C the thermal vibration is so highly excited that the P-O-P bonds appear linear.

The two-fold axis passes through the cation and thus must be one magnetic axis.[18] The other two axis therefore lie in the a-c plane. X-ray work indicates the possibility of C-2, C-m, or C-2/m symmetry, but the esr work reported here shows only one cation site. Hence the C-2/m group was chosen.

On transition from the β to the α phase, axes a and c of the unit cell are roughly doubled. The unit cell now contains 8 molecules and therefore 16 possible sites for the paramagnetic Mn^{++}. The esr technique is sensitive only to the inversion invariant point group symmetry if that is equal or higher than orthorombic. It does not see the translational symmetry elements. The B-centering and centre of symmetry in the point group for α-$Mg_2P_2O_7$ each reduce the number of non-equivalent sites by a factor of 2. Thus we should see four different sites in esr. Further reduction is possible only if one of the magnetic axis of the paramagnetic ion coincides with the b-axis.

The P-O-P bonds are not linear in the α-phase, but bent to an angle of approximately 142°. The cations have undergone a displacement during the transition so that in α-phase they do not superpose on each other in a projection onto the B-face. The two crystallographic cation sites in their respective highly distorted six-oxygen octahedra are very different. In one all the Mg-O bonds lie within 0.06Å of 2.13Å, in the other five of Mg-O bonds lie within 0.05Å of 2.08Å while the sixth is measured to be 3.36Å.

TABLE I [26,27]

$Mg_2P_2O_7$ Crystallographic Data

β-$Mg_2P_2O_7$(95°C) Space Group C-2/m

$a = 6.494 \pm .007$

$b = 8.28 \pm .01$

$c = 4.522 \pm .005$

$\beta = 4.522 \pm .005$

$Z = 2$

α-$Mg_2P_2O_7$ Space Group B-21/c

$a = 13.198 \pm 0.005Å$

$b = 8.295 \pm 0.005Å$

$c = 9.072 \pm 0.005Å$

$\beta = 104.9 \pm .1^\circ$

$Z = 8$

CHAPTER IV

Experimentation

1. Preparation of the Sample

The crystals we used were grown by J. G. Chambers by slow cooling of a melt of $Mg_2P_2O_7$ with a small quantity of $Mn_2P_2O_7$ added. The pyrophosphates were prepared by the decompositions of precipitated Mg NH_4PO_4 and Mn NH_4PO_4 respectively.[35] The crystals thus prepared were quadilateral plates with well defined crystal faces. The concentration is$(Mg_{99.75}\ Mn_{0.25})_2\ P_2O_7$.

2. The Spectrometer

General set-up of the 8mm spectrometer used is shown in the block diagram. A Kepco model 1520B power generator (0 - 1500V.) is employed for the beam voltage. The beam current is about 8ma. A John Fluke model 406 powere generator supplies both the reflector and filament voltage (0 - 500V.d.c. and 6.3 V. a.c. respectively). A rectifier built external to the generator is used to cut down noise by rectifying the latter voltage into a 6 V.d.c. The bias voltage built in this generator could not be used because of polarity problem. A simple diode bridge added to it supplies this voltage (0 - 100V.)

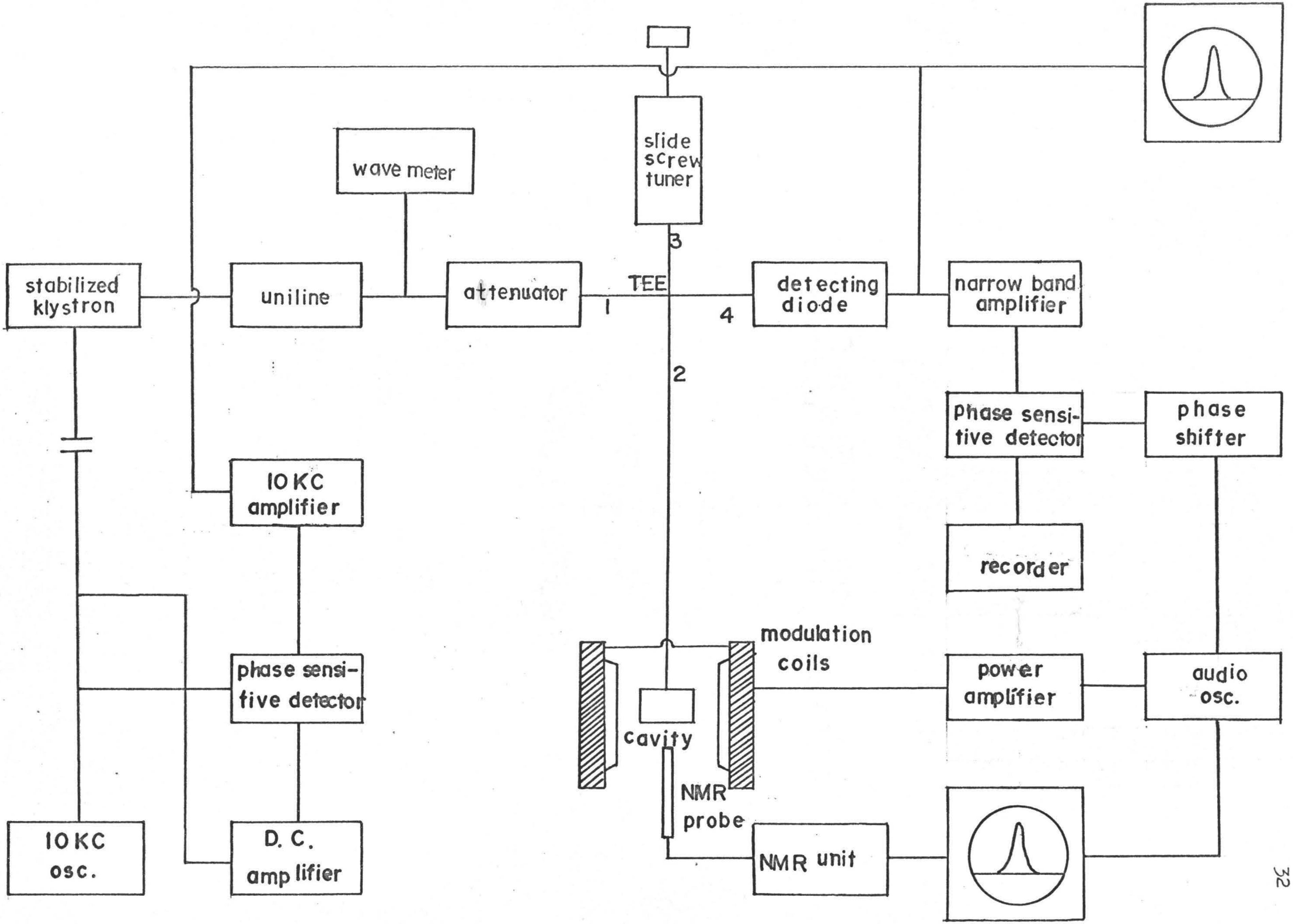

Fig. 2 BLOCK DIAGRAM OF THE 8mm MICROWAVE SPECTROMETER

A EMI type R5146 Klystron is used to generate the microwave power. This reaches arm 1 of the magic tee after passing through a uniline, an adjustable attenuator and a wave metre. Arm 3 terminates in a load with a slide screw tuner. The spectrometer is operated at the resonance frequency of the cavity with the sample in it. When the impedence of arm 2 and 3 are balanced, there is no microwave power reaching arm 4, except the possible noise due to instability of the klyston frequency. This frequency, however, as will be shown, is stabilized by a lock-in loop. The balance between arm 2 and 3 is off set when the sample in the cavity absorbs additional microwave power as the magnetic field sweeps passed the resonance condition. This causes a variation in the microwave power in arm 4, which is proportional to the amount of absorption. A small oscillating field generated by two coils wound around the pole faces modulate this absorption signal at a frequency of 100c/s. The phase of modulation undergoes a change of 180^o as the absorption peak is passed. This absorption signal is detected by a diode mounted at arm 4 and sent directly to an oscilloscope for display in addition to passing through a narrow band amplifier, a phase sensitive detector to a recorder. These modulation coils are wound with 600 turns of No. 26 copper wire and are driven in parallel by a push-pull power amplifier. A Princeton model JB4 compound unit contains the narrow band amplifier, the phase sensitive detector as well as the generator of the 100 cycle modulation signal.

The klystron frequency is stabilized by locking it to the sample cavity. For this purpose a phase sensitive detector is used. A 10 Kc small signal is impressed on the reflector voltage, giving rise to a frequency modulated error signal of 10 Kc at the detection arm. This error signal changes phase by 180° as the klystron frequency passes through that of the sample cavity. Therefore the error signal is converted into a correcting voltage which, after amplification, is sent back to the klystron reflector. The circuit diagram of the phase sensitive detector used is shown in Fig. 3.

A Varian model V-4007 magnet is used with 6" pole faces and 1/2" air gap. The power supply and field sweep system were built by Piczonka[28]. The current fed into the magnet is stabilized to one part in 10,000. A synchronous motor driving a 10 turn helipot in the stabilizer circuit effects the sweeping. The sweeping speed is controlled by varying a resistance in parallel with 1000Ω helipot. For survey work, the field is swept at a speed of 150 gauss/min. while the final data were measured at the slower speed of 85 gauss/min. The separation between two hyperfine lines is about 87 gauss and the filtering time constant of the detecting system is 2 sec. The time that elapses in passing from one hyperfine peak to another is therefore about 30 times the time constant. To eliminate any errors that may arise because of inertia in the recording system, two spectra, one with the magnetic field swept up and the other swept down, were taken for each measurement and the line positions were taken to be the average of the two.

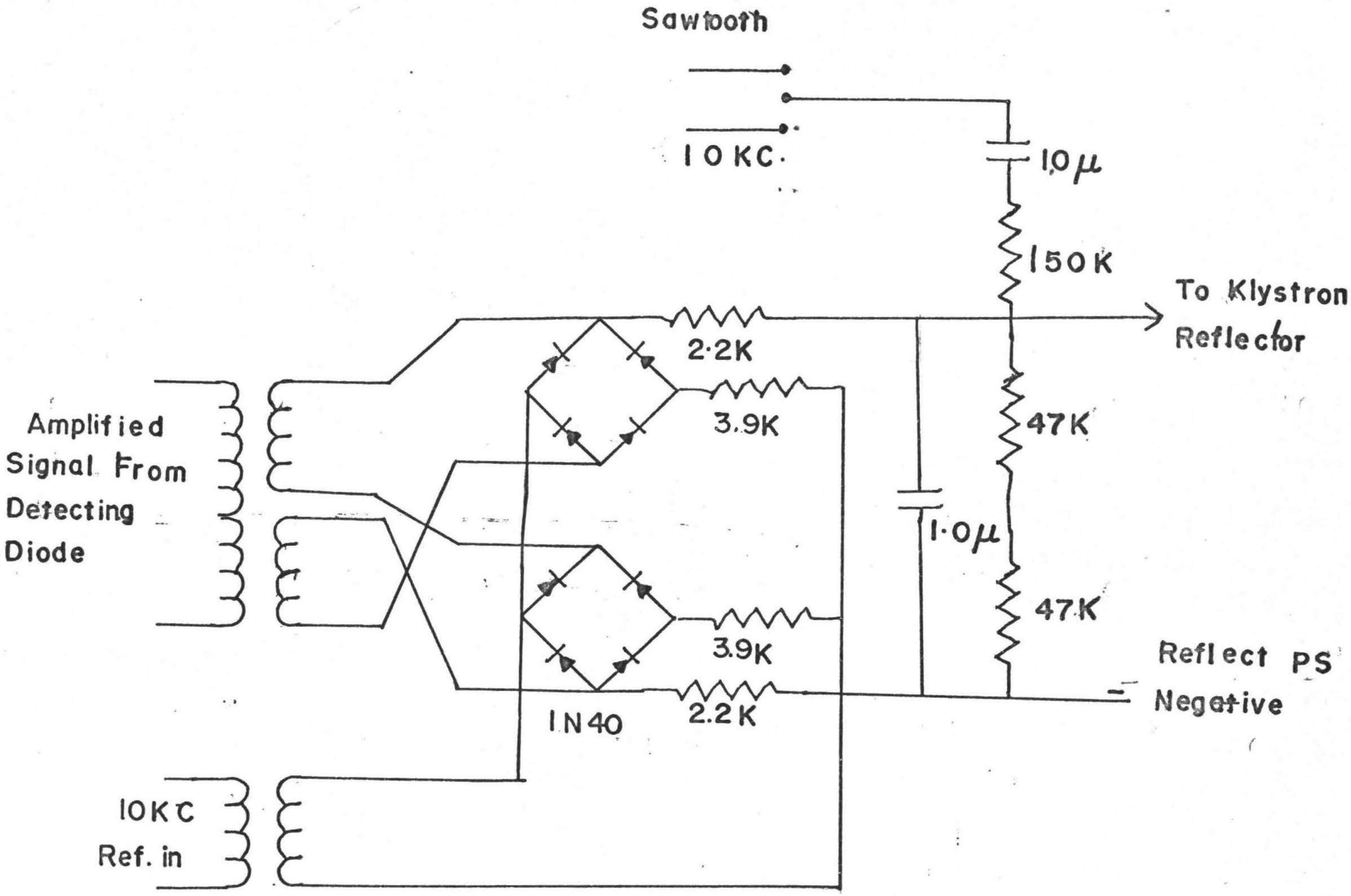

Fig.3 Circuit Diagram of Phase-Sensitive Detector For Klystron Frequency Stabilization

3. Sample Mounting, Temperature Control and Measurement

The rectangular cavity is made out of a piece of wave guide sealed at the end. It has the dimensions of 0.65 x 0.32 x1.63 cm. and operates in the TE_{102} mode. The iris has a diameter of 5/64". The sample is inserted into the cavity through a hole on the narrow side. To avoid serious upset of the cavity Q, the sample holder is made of a 3mm glass tube drawn out to be 0.5mm at the end where the crystal is mounted. A copper-constantan thermocouple is inserted into the holder. At the tip, the crystal, the holder and the thermocouple are glued together with proxyl. This ensures a good thermal contact.

The cavity is placed into an oven made of supramica, which fits tightly, sandwiched between two pieces of asbestos , between the pole faces of the magnet. This reduces the vibration of the cavity. In addition the vibrations of the modulation coil can be a serious nuisance. This is reduced considerably by fitting wood blocks between them.

A small nicrome wire coil wound around the bottom part of the cavity is used as heater. It is supplied by a selenium rectifier bridge. The maximum current obtained is 3 amp. and this produces at the cavity a temperature of 220°C. Since the cavity is small and the dimension of the crystal used must be still samller, we may assume that the temperature of the crystal is homogeneous. A Sola transformer is used to reduce fluctuation of the line voltage and maintain a steady current. Two variacs and a rheostat in series are used to achieve fine control. The e.m.f. on the thermocouple is measured by a thermocouple potentiometer. The temperature determination is estimated to be accurate to 0.5°C. But on sweeping the magnetic field from 7KG to 15KG, there is a systematic decrease of 1°C and vise versa. The reason for this change is not known. Therefore, the temperature of a spectra can be specified to only within ± 1°C. This is important because the determination of the exact temperature of the phase transition depends on the pattern of the whole specta.

4. Alignment of Crystals

The crystals of $Mg_2P_2O_7$:Mn are quadrilateral plates. A preliminary survey showed that a large crystal seriously reduced the cavity Q while too small a crystal did not yield signals strong enough to be detected. Crystals of various sizes were tried and finally two crystals were chosen of size 1mm lengthwise and 1/2mm in thickness. This represented a compromise of the two factors mentioned above. It was known that the two-fold b-axis lies on one flat surface. Rotating crystal pictures were taken by X-ray to determine this axis. By the consideration of symmetry, this has to be one of the magnetic axes in the β-phase.[18] The sample can only be rotated about that one axis which is parallel to the pole faces in the esr experiment. Therefore two crystals were necessary in order to obtain complete data. One crystal could be rotated about the b-axis and the other about an axis perpendicular to the two-fold axis.

To find the z and x axis in the high temperature phase, the crystal was rotated about the b-axis (which is designated the y-magnetic axis) and esr spectra were taken at different angular positions at 5° interval. The angular position can be set as accurate as 1°. Positions of the ± 3/2 ⟷ ± 1/2 transitions were plotted against the angular position of the magnetic field in Fig. 4. The curve shows two maximum separations 90° apart. The two additional axes lie parallel to these directions. This follows from the properties of a symmetric tensor. The spectra merged together at 55° from one axis and repeats itself after 180°. These evidences showed that we were actually rotating about a two-fold axis.

To investigate the y-axis, a second crystal was carefully inserted into the cavity so that the b-axis as determined by X-ray was as close to parallel to the magnetic field as possible. It was then rotated about an axis perpendicular to the b-axis. Spectra were taken periodically in angle until we got maximum splittings.

5. Magnetic Field Measurement

For survey work a rotating coil gaussmeter was used to measure magnetic field. Values as high as 15 kilogauss could be measured to an accuracy of 0.2 kilogauss. For accurate measurement, the NMR probe with lithium chloride solution is used. This enables measurement of magnetic field as high as 13.5 kilogauss. Calibration points of magnetic field were made at intervals of about 150 gauss as the spectra was traced out.

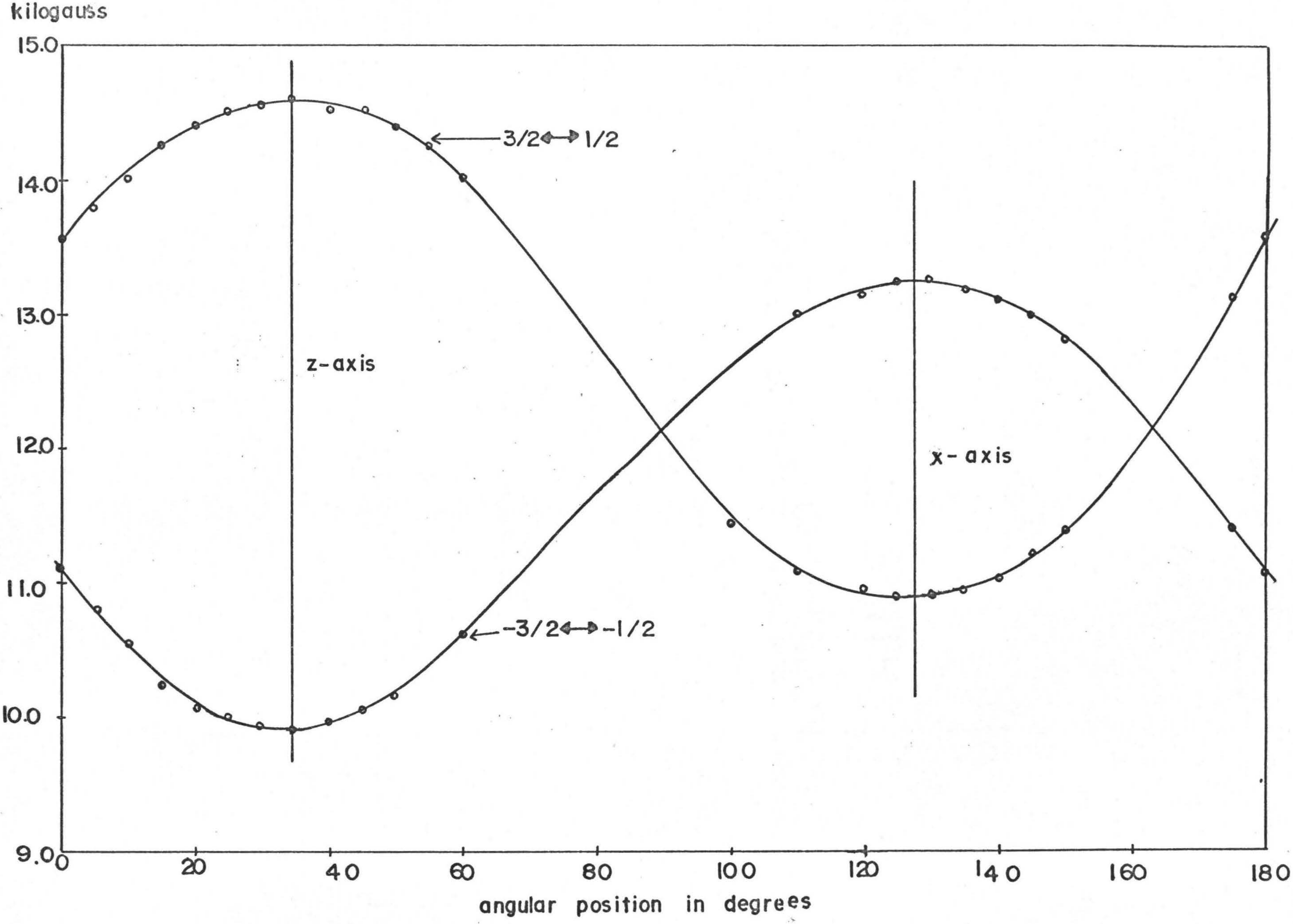

Fig. 4 Variation of Line Position For Transitions 3/2 ↔ 1/2 and -3/2 ↔ -1/2 Against Angular Position When Crystal Is Rotated About The b-axis

This was done by watching the NMR signal on an oscilloscope and mark was made on the recording chart as this signal crosses the centre and at the same time one measured the frequency of the NMR oscillator with a Bendix Radio BC 221-M beat frequency oscillator. The magnetic field was measured with an error of ± 2 gauss.

CHAPTER V

Results

1. The Spectra and Resolution of the Hyperfine Structures

For survey work spectra were taken from 7 kilogauss to 15 kilogauss and at about 80°C. Each spectrum revealed five fine structure lines except for that taken with the magnetic filed parallel to the z-axis where the second upper **satellite** occurs at too high a magnetic field to be seen. These spectra show that only one esr active site is occupied by Mn^{++} in β-$Mg_2P_2O_7$.

At room temperature, spectra taken **with the magnetic field parallel** to high temperature x-axis and y-axis show groups of continuous and multi-superposed lines in the range between 9 kilogauss to 14.5 kilogauss. Hence we conclude that a significant shift occurs in the axes of the magnetic ellipsoid in passing to the α-phase. With H parallel to the z-axis of the β-phase, the following groups of lines are seen.

Number of hyperfine lines	Approximate centre of the group
6	13.3(KG)
12	12.3
6	11.3
6	10.3
6	8.5
6	5

Thus it appears that in the low temperature phase there are two non-equivalent crystal sites taken up by Mn^{++} in α-$Mg_2P_2O_7$.

For reasons mentioned above, no line above 13.5 kilogauss could be measured accurately. The following lines at the axes indicated have been carefully measured, all at three different temperatures (74°C, 84°C and 94°C):

Axis	Fine Structure Lines Measured
x	U_1, C, L_1, L_2*
y	U_1, C, L_1+, L_2*
z	C, L_1*, L_2*

Here C stands for the central line that is near the g = 2 value for magnetic field. L_1 and L_2 are the lower first and second satellite and U_1 the upper first satellite The asterisk* indicates the line does not have its hyperfine structure resolved at all three temperatures while the dagger + means that hyperfine structure is seen to resolve only at 94°C.

One spectra at z-axis is taken at 174°C. Here the line L_{1z} and U_{1z} are resolved while L_{2z} still is not.

2. Phase Transition Temperature of $Mg_2P_2O_7$:Mn^{++}

Little change was noted in the pattern of lines when esr spectra were taken at different temperatures within the two intervals between room temperature and 58°C and between 63°C and 200°C. The spectra in these two temperature ranges are different. To determine the transition temperature accurately, and to check the reversibility of changes in the crystal, data were taken within the interval 58°C-63°C for both decreasing and increasing steps of 1°C. At the z-axis, the high temperature spectra appears abruptly at 59.5°C, superposed on the low temperature spectra. At 62.5°C, the low temperature spectra disappears. The details of changes in spectra from 58°C to 64°C are shown schematically in Fig. 6. The lines represent fine structures. The numbers appearing under each line shows the number of hyperfine lines there are in the group. The height of these lines represents their relative intensity as well as variation in the latter with temperature. A line represented by a T is a very broad line not resolved at all. Unfortunately, no investigation has been made for magnetic field below A in this temperature range. Two consecutive spectra taken four hours apart at 61.5°C are the same. This indicates that the coexistance of two phases seen on the z-axis spectra is probably not due to an hysteresis effect.

3. Determination of Spin-Hamiltonian Parameters

Since the parameter D is expected to be large it is the most influential term in equations (5). An esr experiment itself does not suffice to determine the absolute signs of the parameters. These constants may be determined from a knowledge of the susceptibility or the specific heat or relative line intensities, all at low temperature, or the susceptibility anisotropy. However, the spectra give information

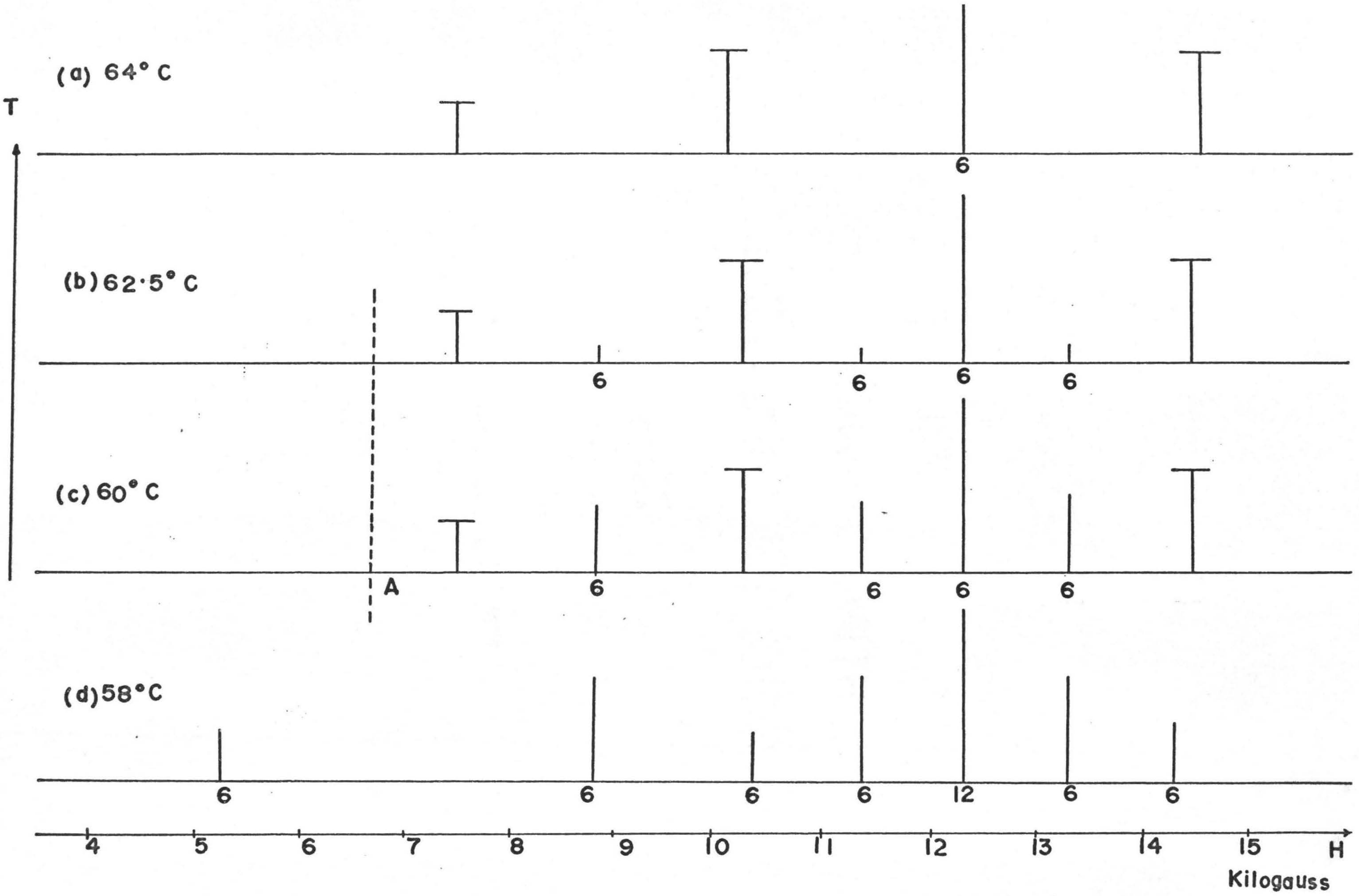

Fig.6 Schematic Diagram of Changes In The Spectra With Temperature When H‖ z-axis

on the signs of A/D. For $A/D > 0$ the extreme separation of a group of hyperfine lines is larger at the low field end than at the high field. The converse is true for $A/D < 0$[30]. Our data show that $A/D > 0$ (Table II). Positive values of A for Mn^{++} have hitherto not been reported. Hence, we probably have a negative D.

Assuming a negative D, the positions of fine structure lines relative to magnetic field can be obtained from equations (5). Furthermore, for negative A, hyperfine lines of larger m_I fall at higher magnetic field. These results are expressed schematically in Fig. 5.

$D < 0$

Axis	Fine Structure Lines				
z	(-5/2 → -3/2)	(-3/2 → -5/2)	(-1/2 → 1/2)	(1/2 → 3/2)	(3/2 → 5/2)
x	(5/2 → 3/2)	(3/2 → 1/2)	(1/2 → -1/2)	(-1/2 → -3/2)	(-3/2 → -5/2)
y	(5/2 → 3/2)	(3/2 → 1/2)	(1/2 → -1/2)	(-1/2 → -3/2)	(-3/2 → -5/2)

$\xrightarrow{\qquad\qquad\qquad}$

H

$A < 0$

Hyperfine Structures

m_I	-5/2	-3/2	-1/2	1/2	3/2	5/2

$\xrightarrow{\qquad\qquad\qquad}$

H

Figure 5

The hyperfine interaction tensor A with components A_x, A_y, A_z is obtained by analysing all the resolved lines in the spectra taken along the respective axis. From equation (7), it can be derived that the separation d, between two neighbouring lines can be written as $d = -A + x \frac{A^2}{H_o}$ where x is in every case we had considered an integer. Suitable combination of d's can be chosen to eliminate the second order term and A may be obtained directly. The value of A for all the temperatures considered are listed in Table II.

The fine structure position is obtained by adding the quantity $\frac{17}{4} \frac{A^2}{H_o}$ to the mean position of the third and forth line in the group. For $A = -87$gauss, and $H_o = 12271$ gauss, $\frac{17}{4} \frac{A^2}{H_o} = 2.6$ gauss.

The centre of an unresolved fine structure cannot be determined very accurately because the difficulty in determining the true base line and hence the true absorption peak. Therefore, only the resolved lines are used in determination of D and E. The process used is described below. From here we shall refer to the centre of a fine structure line obtained by the method described above simply as the line for brevity. The line C at z-axis is first obtained. It is taken as the first approximation of H_o in later calculations. From equations (5 and 6) the difference between line U_1 and C for the x and y axis can be written respectively as

$$\begin{matrix} d_x \\ d_y \end{matrix} = \pm 3E - D - \frac{0.75}{H_o}D^2 \mp \frac{1.5}{H_o}DE - \frac{4.125}{H_o^2}D^3 \pm \frac{4.125}{H_o^2}D^2E + \frac{1.6875}{H_o^3}D^4 \mp \frac{6.75}{H_o^3}D^3E \qquad (17a, b)$$

Equations (17a,b) were solved simultaneously by approximation, using the magnetic field of the line C_z as H_o. The value of D and E were then substituted into equations (5 and 6). Values of H_x and H_y were obtained from the position of U_{1x}, C_x, and L_{1x} and U_{1y}, C_y (and also L_{1y} at 94°C) respectively. These values were now used as H_o's in equations (17a,b) and new values of D and E were calculated. This cycle was repeated for as many times as was necessary to make the error in the approximation smaller than the experimental error. At the end of this process, we have obtained values of D,E, H_x and H_y. H_z was then obtained by substituting for D and E in the equation of C_z. Value of components for the g tensor was calculated from the respective value of H_x, H_y and H_z, using the average microwave frequency. Results of these calculations are listed in Table III.

TABLE II

74°C

	TRANSITION	m_I	Position of Lines (gauss)		
			x	y	z
		5/2	13499*	13462	
		3/2	13426	13371	
		-1/2	13335	13290	
U_1	$\mp$ 1/2 → $\mp$ 3/2**	-1/2	13248	13193	
		-3/2	13166	13112	
		-5/2	13086	13048	
		5/2	12229	12228	12495
		3/2	12144	12144	12403
		1/2	12055	12047	12313
C	± 1/2 → $\mp$ 1/2	-1/2	11971	11962	12224
		-3/2	11833	11875	12134
		-5/2	11799	11757	12047
		5/2	11129		
		3/2	11012		
		1/2	10927	10937	9916
L_1	± 3/2 → ± 1/2	-1/2	10848		
		-3/2	10753		
		-5/2	10675		
L_2	± 5/2 → ± 3/2		9994+	10013	7576

* A resolved line has an error of ± 2 gauss

+ An unresolved line is accurate to ± 20 gauss

** The upper sign for x and y axis, the lower for z-axis

TABLE II (continued)

84°C

TRANSITION		m_I	Position of Lines (gauss)		
			x	y	z
U_1	$\mp 1/2 \longrightarrow \mp 3/2$	5/2	13426	13414	
		3/2	13405	13334	
		1/2	13317	13253	
		-1/2	13228	13160	
		-3/2	13144	13068	
		-5/2	13064	12987	
C	$\pm 1/2 \longrightarrow \mp 1/2$	5/2	12232	12190	12497
		3/2	12145	12100	12400
		1/2	12055	12015	12310
		-1/2	11971	11927	12214
		-3/2	11884	11840	12124
		-5/2	11803	11756	12034
L_1	$\pm 3/2 \longrightarrow \pm 1/2$	5/2	11151		
		3/2	11053		
		1/2	10958	10929	9948
		-1/2	10870		
		-3/2	10783		
		-5/2	10705		
L_2	$\pm 5/2 \longrightarrow \pm 3/2$		9986	9991	7598

TABLE II (continued)

94°C

TRANSITION		m_I	Position of Lines (Gauss)		
			x	y	z
U_1	$\mp 1/2 \longrightarrow \mp 3/2$	5/2	13499	13375	
		3/2	13426	13300	
		1/2	13335	13205	
		-1/2	13248	13129	
		-3/2	13166	13039	
		-5/2	13086	12953	
C	$\pm 1/2 \longrightarrow \mp 1/2$	5/2	12229	12174	12490
		3/2	12144	12088	12398
		1/2	12055	11996	12305
		-1/2	11971	11908	12214
		-3/2	11833	11821	12125
		-5/2	11799	11735	12039
L_1	$\pm 3/2 \longrightarrow \pm 1/2$	5/2	11129	11122	
		3/2	11012	11036	
		1/2	10927	10943	10055
		-1/2	10848	10862	
		-3/2	10753	10769	
		-5/2	10675	10680	
L_2	$\pm 5/2 \longrightarrow \pm 5/2$		9994	9980	7595

TABLE III

Temperature	74°C	84°C	94°C
A_x	88 ± 2	87 ± 2	87 ± 2
A_y	89 ± 2	86 ± 2	88 ± 2
A_z	88 ± 2	93 ± 2	90 ± 2
D	-1218 ± 4	-1208 ± 4	-1186 ± 4
E	7 ± 2	4 ± 2	2 ± 2
g_x	2.0084 ± 0.0020	2.0080 ± 0.0010	2.0087 ± 0.0020
g_y	2.0084 ± 0.0020	2.0139 ± 0.0010	2.0185 ± 0.0020
g_z	2.0033 ± 0.0020	2.0048 ± 0.0010	2.0047 ± 0.0020

$\bar{\nu}$ = 34.420 ± 0.005 Megacycle

CHAPTER VI

Discussions

Values for spin-Hamiltonian parameters are listed in Table III. The average D value at three temperatures 74°C, 84°C, and 94°C (-1205 gauss), is comparable to that obtained for $Zn_2P_2O_7:Mn^{++}$ (D = -1103 gauss). The D value for $Mg_2P_2O_7:Mn^{++}$ would be expected to be larger, if we assume that the amount of distortion caused by Mn^{++} in the two host crystals are about the same. Since Mg has a smaller atomic radius than Zn, the decrease in atomic separations would give rise to a stronger crystal field. Any serious attempt to calculate D theoretically is hampered by the facts that (1) the functional relation between D and the axial field component Y_2^0 is not at all clear, as was discussed in Chapter II, (2) the ionic model may not be an adequate approximation for the estimation of the electric field, and (3) the distortion Mn^{++} imposes on the host crystal is not known. The error in the value of D at the three temperatures have been estimated from the combined error in the line positions from which it is calculated. The variation of D with temperature is not surprising, as the work of Roy et al[32] indicates a considerable change in volume across the transition.

The value of E cannot be measured accurately, but clearly is small in magnitude. From this we can conclude that the symmetry at the Mn^{++} is essentially axial. A similar conclustion was obtained in the case of $Zn_2P_2O_7:Mn^{++}$.

The hyperfine structure tensor $\overleftarrow{A}$ stays practically constant throughout the temperature range and no reason for the anisotropy can be proposed. The value of $\overleftarrow{g}$ tensor reported here not only deviates more than usual from the free ion value, but also are anisotropic. We cannot see any evident functional relation of it with temperature.

In evaluation of H_x and H_y from the experimental value of D and E, a substantial deviation is obtained in the value derived from different fine structure lines. The average deviation is 10 gauss. This is expressed as the error in the value for the g tensor components. This is considerably larger than our experimental error (± 2 gauss). Upon subtracting (5.2) from (5.3), one obtaines an expression not containing a first order term in E and thus is most convenient for the evaluation of D. Since the line labelled L_{1z} is not resolved in our experiment, our error is bound to be increased considerably. Also, it has been shown that to describe the problem completely, more parameters are needed than that in the spin-Hamiltonian. There are reports of descrepence of experimental data from a spin-Hamiltonian parameter fitting as much as 5 to 10%[36]. Since the zero field splitting is large, one would not be surprised by a difference in the splittings between levels ± 1/2 and ± 3/2 as compared to that between levels ± 3/2 and ± 5/2. Thus, one should use an extended spin-Hamiltonian. However, broadness of the lines would probably preclude any definite conclusion.

There is evidence of line broadening near the transition temperature. The line labelled L_{1y} is not resolved at 74°C and 84°C, but is seen to resolve at 94°C. The lines L_{1z} and U_{1z} are seen to have resolved only at 174°C. These lead one to conclude that there is greater inhomogeneity in the crystal field at different individual sites near the transition. However, these inhomogeneities apparantly persist far beyond the temperature that can be assigned for the transition in either the X-ray or esr experiment.

It was confirmed that the z-magnetic axis lay roughly parallel to the $(10\bar{1})$ crystallographic direction in the β-phase, and that this axis rotated by 20° towards the b_1 reciprocal lattice vector upon passing through the transition. A precise measurement was not made because of the difficulties of transferring the crystal from the cavity to the goniometer head for the X-ray experiment. One can remark, however, that the z-axis lies roughly parallel to the long Mg-O_{III} bond.

The phase transition observed here occured 8°C earlier than that reported by specific heat measurement[33] and X-ray work on power crystal of $Mg_2P_2O_7$[32]. This might be accounted for by the presence of Mn^{++} in the crystal if the phase change involves very small difference in free energy. There havebeen examples where impurities in a crystal drastically changes the phase transition temperature of the host, e.g. ferro-electric -paraelectric transitions of Ba Ti O_3 is changed by

140°C at % when Fe_2O_3 is added to it.

A gradual change from α to β phase is observed here to occur within a much narrower range of 3°C instead of 20°C as seen by specific heat experiment. Although the line broadening does extend further in temperature. Recent specific heat measurement here confirms that our samples show a much narrower anomaly[29]. Across this phase transition, the symmetry of the crystal is increased from $B\text{-}2_1/c$ to C-2/m through the addition of the symmetry elements (0,0,1/2) and an inversion. In addition, there is the evidence for the coexistance of the two phases between 59.5°C to 63°C. The y-magnetic axis does not lie parallel to the 2_1 axis in the α-phase but lies along the two-fold axis in the β-phase. This coexistance of two phases in a one component system is precluded by the Landau-Lifshitz theory of second order phase transition, because the minimum Gibb's free energy function of either phase does not exist at all beyond the transition point. Hence there cannot be any supercooling or superheating effect. However, if Φ involves additional variables besides the order parameter η, such a coexistance of both phases is possible[38]. A thorough theory for such cases is not yet available.

X-ray work on single crystal of $Mg_2P_2O_7{:}Cu^{++}$ [26,27] has seen a distinct β' phase, probably of symmetry C-m, between the α and β phases and possibly coexisting with the latter phase in some small range of temperature. No evidence has been found in these experiments for coexistance of β' and α or β and α phases.

The space group B $2_1/c$ assigned to the low temperature phase according to X-ray crystallography would require four non-equivalent esr active sites, two from one molecule of $Mg_2P_2O_7$ and another two generated from the former by the screw axis 2_1. But at a position where the magnetic field is parallel to the high temperature z-magnetic axis, esr sees only two different sites. This descrepency may be due to the fact that the esr experiment fails to resolve the two sites related by the 2_1 axis at this particular position. Hence it is likely that the two sites manifest a broadening of the lines rather than the distinct resolution of two spectra. Another possible explanation is that Mn^{++} substitute the Mg^{++} sites selectively. But this is very improbable because at the melting point of $Mg_2P_2O_7$ the entropy of the crystal is so large that there should be scarcely any chance of ordering while the diffusion of the Mn^{++} should cease somewhat near the melting point.

Also, to attain coherance between the X-ray and esr results, we have to admit that somehow each of the techniques missed one of the coexistance of phases. ESR sees only the α-β' coexistance and X-ray crystallography sees only the β-β' coexistance. And, since the space group of the β' phase, probably C-m, is of lower symmetry than the B-$2_1/c$ of the α-phase (with the 2_1 axis lacking), the α-β' transition cannot be a λ-transition and must be a first order one. This would require the esr spectra to change abruptly at the α-β' transition. But quite contrary to this, the α-phase spectra persists through this transition temperature. Furthermore, because the space group C-m requires two non-equivalent esr sites, the esr experiment should see in the intermediate temperature range a superposition of two spectra on each other, one with a single site and the other having two distinct sites. The β'-β transition would be continuous and beyond this only the single site spectrum with space group C-2/m would be seen. There is a possibility, although remote, that the descrepency arises from the fact that $Mg_2P_2O_7:Mn^{++}$ was studied by esr and $Mg_2P_2O_7:Cu^{++}$ by X-ray.

X-ray crystallography has also revealed the spiral arrangement of the electric dipole associated with the bent P-O-P group in the α-phase. **In the β-phase, these dipoles are randomly oriented. This randomness can either be statistical or may be due to thermal motion of the dipoles.** It might well be conjectured that such rearrangement is in fact the order-disordering effect that triggers the phase transition, although the broaden lines indicate a disordering that persists quite far above the transition point.

The phase transition phenomena we have observed here is very complicated and even a satisfactory qualitative description is not feasible. The mechanism for the phase transition as well as the paradox of two phases coexisting can only hope to be explained by a statistical theory which takes into account microscopic effects in the crystal besides that of order-disorder. However, careful esr study on α-$Mg_2P_2O_7:Mn^{++}$ and $Mg_2P_2O_7:Cu^{++}$ as well as X-ray crystallographic study of $Mg_2P_2O_7:Mn^{++}$ are desirable. These further experiments would possibly provide data for exact number of sites in the α-phase, and the influence of impurities on the structure of host crystal as well as phase transition temperatures.

With so little data available, we cannot get at the physical nature of S-state splitting. More esr data on various series of isostructural crystals are necessary before we can hope to reach at a reliable functional relation between D and Y_2^o and to determine the dependence of the latter on crystal structures. In addition, if we can excite enough paramagnetic ions into some excited states and then investigate, with esr, the splitting of them in the crystal field, we may also get some insight into what is really happening to the S-state.

REFERENCES

1. E.U. Condon and G. H. Shortley, The Theory of Atomic Spectra, Cambridge University Press (1935).
2. H. A. Bethe, Ann. Physics, [5] , 3, 133 (1929).
3. B.R. Judd, Operator Technique in Atomic Spectroscopy, McGraw Hill (1963)
4. M. Tinkham, Group Theory and Quantum Mechanics, McGraw Hill (1964)
5. K.W.H. Stevens, Proc. Phy. Soc. (London), A65, 209, 1952
6. A. Abragam and M.H.L. Pryce, Proc. Roy. Soc. (London) A205, 135 (1951)
7. B. Bleaney, and K.W.H. Stevens, Rep. Progr. Phys. 16, 108 (1953)
8. G. J. Kynch, Trans. Faraday Soc. 33, 1402, (1937)
9. M.H.L. Pryce, Phy. Rev. 80, 1107 (1950)
10. H. Watanabe, Prog. Theoret. Phys. 18, 405, (1957)
11. J. R. Gabriel, D. E. Johnston, and M.J.D. Powell, Proc. Roy. Soc. 246, 503, (1961).
12. W.J. Nicholson and G. Burns, Phy. Rev. 129, 2490 (1963)
13. A. Abragam, Phys. Rev. 79, 534, (1950)
14. V. Heine, Phys. Rev. 107, 1002 (1957)
15. T.H. Wood and G.W. Pratt, Phys. Rev. 107, 995, (1957).
16. K. D. Bowers and J. Owens, Repts. Prog. Phys. 18, 304 (1955)
17. Y. Yoleozawa and Y. Kerzumata, J. Phys. Soc. Japan 16, 694 (1961)
18. J. G. Chambers, Ph.D. Thesis, McMaster University, 1964.
19. W. Low, Solid State Physics, Sup. Vol. 2, 1962
20. G. F. Rozter and H. Statz, Phy. Rev. 115, No. 6, 445 (1959)

21. M.E. Rose, Angular Momentum, John Wiley and Sons Inc. New York (1957)

22. H. Statz and G. F. Koster, Phys. Rev. 115, No. 6, 1568 (1959)

23. N.J.C. Grant and M.W.P. Strandberg, J. Phys. Chem. Solids, 25 635, (1964)

24. L.D. Landau and E.M. Lifshitz, Statistical Physics, Addison Wesley (1958)

25. C. Calvo, to be published (1965)

26. C. Calvo, private communication

27. C. Calvo, to be published (1965)

28. W.A. Pieczonka, Master Thesis, 1957

29. C. V. Stager, private communication

30. W. Low, Solid State Physics, Sup. Vol. 5, 1962

31. J. G. Chambers, W. R. Datars and C. Calvo, J. Chem. Phys. 41, 806 (1964)

32. R. Roy, E. T. Middlesworth and F. A. Hummel, Am. Mineral 23, 45j (1948)

33. F. L. Oetting and R. A. McDonald, J. Phys. Chem. 67, 2737 (1963)

34. R.J. Bersohn, Chem. Phys. 29, 362, (1958)

35. W. Rieman, J.D. Neuss and B. Naiman, Qualitative Analysis, McGraw Hill, 1942

36. K.A. Muller, Helv. Phys. Acta 31, 173 (1958)

37. R. T. Arnold and A.L. Stanford, Jr., J. Chem. Phys. 41, 1520 (1964)

38. A.R. Ubbelohde, Quart. Rev., 11, 246 (1957)